

# CHAPTER FIVE

## NEW SIGNAL PROCESSING METHODS FOR ESTIMATION OF PULSAR ROTATION MEASURE

As discussed in Chapter 1, most of the known pulsars are sources of highly linearly polarized radiation. The position angle of the linear polarized component changes as a function of longitude within the pulse in a manner that depends on the geometry of the spin axis and magnetic poles of the pulsar relative to the observer's line of sight (Radhakrishnan and Cooke, 1969). At a given longitude the average polarization seems to have a good long term stability in most cases. By folding the pulses over its period it is possible to estimate reliably the apparent position angle of the radiation of different longitudes within the pulse. However, Faraday rotation in the interstellar medium and the ionosphere rotates the plane of linear polarization by different amounts at different frequencies within the band as described in chapter 1. The extent of rotation is determined by the rotation measure (RM) given by equation.(5.1). It is clear from this equation that by measuring the polarization angles in different frequencies spanning a sufficiently wide band one can estimate the RM.

$$\theta = RM\lambda^2 \quad (5.1)$$

where  $\lambda$  is the observed wavelength.

### 5.1. RM Measurements with a Single Polarization Telescope:

Usually polarization measurements use antennas with dual orthogonally polarized feeds. By measuring the stokes parameters across the spectrum it is possible to find the polarization angle at different frequencies. At lower radio frequencies, the Faraday rotation of the position angle becomes large enough to measure the differential rotation within reasonable band widths. In addition, the pulsar signal is generally stronger. at lower frequencies although at very low frequencies the strong galactic background radiation seriously affects the sensitivity in these measurements. Thus it is essential to choose a suitable observing frequency, use large bandwidths and highly sensitive telescopes to achieve the required precision in such measurements. A number of pulsars for which rotation measure has been observationally estimated are only about 180 (Taylor & Manchester, 1993) out of about 600 known pulsars. Most of these 180 pulsars are strong sources and hence relatively easier to study. To extend such measurements to weaker pulsars, telescope of very large dimension operating at suitable frequencies are required. Many telescopes may have large collecting area, but a single linear polarization. An indirect way can be used for studying the linear polarization properties in some cases even with a single linear polarization telescope which has a large collecting area. The basic principle involved in this type of measurements is as follows:

For the purpose of simplifying the following discussion, we can assume that the interstellar medium and the ionosphere are stationary over the period of observation and the time-varying effects of these media

are discussed later. When a 100% linearly polarized wave is incident on a linearly polarized antenna, the amount of power received by the antenna from the wave depends, among other things, on the angle  $\zeta$  between the direction of polarization of the wave and the orientation of the antenna feed as

$$P_{\text{received}} = \frac{P_{\text{lin}}}{2} [1 + \cos(2\zeta)] \quad (5.2)$$

where  $P_{\text{lin}}$  is the linearly polarized, incident power. The incident polarization vector rotates by different amounts at different frequencies within the observed bandwidth due to the Faraday rotation in the medium between us and the source. Then, even though the power radiated by the pulsar at those frequencies were same, the power received by a linearly polarized telescope through a total power spectrometer would therefore show a modulation across the band as shown in figure (5.1), of the form given by

$$P(f, + i\Delta f) = A_0 + A_1 \cos \left\{ 2 \left( \zeta + \left( \frac{RMc^2}{(f_L + i\Delta f)^2} \right) \right) \right\} \quad (5.3)$$

where  $f_0$  is the lower edge-frequency of the spectrum,  $\Delta f$  is the width of each frequency channel, "i" is the channel number,  $A_0$  is the average intensity,  $A_1$  is the magnitude of linearly polarized power,  $\zeta$  is the "true" position angle of radiation relative to the antenna's polarization angle, before Faraday rotation and the last term is the total Faraday rotation ( $\theta_i = RM\lambda_i^2$ ). The depth of modulation depends on the fractional linear polarization. In general, the pulsar radiation is partially polarized. In such cases, by observing this modulation in the spectrum of the received radiation, the following conclusions can be drawn:

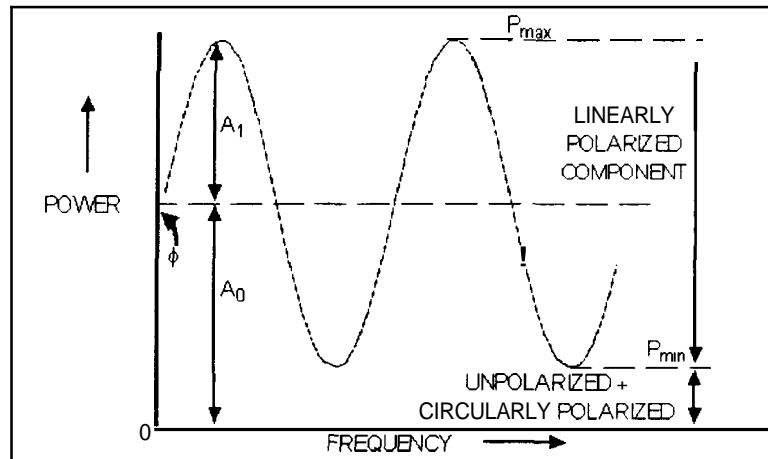


Fig 5 1 Power spectrum modulation due to Faraday rotation in a Linearly polarized, single polarization telescope

1. The degree of linear polarization can be determined from measuring the depth of modulation, calculated as

$$d_l = \frac{P_{\text{max}} - P_{\text{min}}}{P_{\text{max}} + P_{\text{min}}} = \frac{(2 A_1)}{(A_0 + A_1)} \quad (5.4)$$

where  $P_{\text{max}}$  and  $P_{\text{min}}$  are the maximum and minimum values of the apparent spectral power contribution, respectively.

2. By measuring the bandwidth  $B$  over which the modulation completes  $K$  cycles, the Rotation Measure can be estimated as

$$RM = \frac{K\pi}{c^2} \left[ \frac{1}{f_L^2} - \frac{1}{(f_L + B)^2} \right] \quad (5.5)$$

where  $c$  is the velocity of light and  $f_L$  is the lowest frequency of this band.

3. The starting phase of this modulation  $\Phi$ , will shift as a function of the longitude within the pulse, owing to the intrinsic sweep of the position angle during the rotation of the pulsar. One can calculate the angle  $\theta$  by which the polarization vector has been Faraday rotated at a given wavelength  $\lambda$  by using the estimated RM. Then, the position angle of the polarization vector with respect to the polarization angle of the telescope can be estimated as

$$\zeta = \frac{\Phi}{2} - \left( \frac{RM c^2}{f_L^2} \right) \quad (5.6)$$

4. Knowing the dispersion measure (DM in  $PC \text{ cm}^{-3}$ ) and the rotation measure (RM in  $\text{rad m}^{-2}$ ), the mean magnetic field component along the line of sight can then be calculated from the relation

$$\langle H \rangle = 1.235 \left[ \frac{RM}{DM} \right] \quad (\mu\text{Gauss}) \quad (5.7)$$

This method has been put to use earlier (Sulemanova et.al. 1988) for polarization measurement of 18 pulsars. However, the model used to fit for the rotation measure assumes a progress in the modulation phase with frequency of the form

$$\phi_i \propto \frac{2\pi f_i}{i\Delta f} \quad (5.8)$$

where  $f_i$  is the frequency of the  $i^{\text{th}}$  spectral channel and  $\Delta f$  is the channel bandwidth. However, the actual phase progression is of the form

$$\phi_i \propto \left( \frac{2RMc^2}{(f_L + i\Delta f)^2} \right) \quad (5.9)$$

This non-linearity is the progression of modulation phase across the band to be taken into account while observing over large bandwidth or for pulsars which may have large RM, to avoid significant errors in RM estimation. Two new methods (presented below) were developed to fit for RM.  $\zeta$ ,  $A_0$  and  $A_1$  taking into account the non-linearity of equation(5.9).

## 5.2. Auto-Correlation Domain Processing:

Step 1: Linearization of modulation phase :

The argument of the cosine term in equation (5.3) has a non-linear (inverse square) dependence on the frequency of observation, while, usually the observed data corresponds to samples obtained at equal frequency intervals in conventional spectrometer type receivers. The spectrum can be resampled in a suitable (non-uniform) manner such that the argument varies linearly with the new pseudo-frequency indices. This operation makes the modulation appear as that of a pure sinusoidal wave. This "linearization" simplifies the analysis of the data and enable the use of linear methods such as Fourier Transforms, to search and

study the possible periodicity. The transformation is such that the total phase excursion of the modulating signal is same both before and after linearization. This can be achieved by assuming that the initial phase gradient (at lower frequency edge of the band) before and after linearization to be same, and then resampling the raw power spectrum so as to compress the non-linear modulation into a simple sinusoidal form. The values at the new indices may be obtained by interpolating the values of the raw data. The true phase of a given channel (say,  $i^{\text{th}}$ ) may be expressed as

$$\phi_i = a\lambda^2 = \frac{ac^2}{(f_L + i\Delta f)^2} \quad (5.10)$$

where 'a' is a constant co-efficient (equal to the RM), c the velocity of light,  $f_L$  is the lowest edge frequency of the observed band,  $\Delta f$  is the bandwidth per spectral channel. After linearization of phase, a new sequence is obtained, where the phase at any bin (say  $j^{\text{th}}$ ) is in linear progression relative to that at the lowest frequency of the band, related as

$$\phi_j = k + (b \cdot j \cdot \Delta f) \quad (5.11)$$

where b is another constant co-efficient, k is the modulation phase in the lowest frequency channel. With two constraints ( $i = j$  and  $\phi_i = \phi_j$  for  $j = 0, 1$ ) the two expressions can be related as follows:

$$\text{setting } i = j = 0, \text{ we get } k = \frac{ac^2}{f_L^2} \quad (5.12)$$

setting  $i = j = 1$  and using the value of k, we get

$$\frac{b}{a} = \frac{c^2}{\Delta f} \left( \frac{1}{(f_L + \Delta f)^2} - \frac{1}{f_L^2} \right) \quad (5.13)$$

and in general for any index i,

$$\frac{ac^2}{f_L^2} + (j \cdot b \cdot \Delta f) = \frac{ac^2}{(f_L + i \cdot \Delta f)^2} \quad (5.14)$$

Using the above equations, the new index j can be calculated as

$$j = \frac{K_1}{(f_L + i \cdot \Delta f)^2} - K_2 \quad (5.15)$$

$$\text{where } K_2 = \frac{(f_L + \Delta f)^2}{(f_L^2 - (f_L + \Delta f)^2)} \text{ and } K_1 = K_2 \cdot f_L^2 \quad (5.16)$$

In the range of j corresponding to the limits  $i = 0$  &  $i = N_{\text{ch}}$ , the index j is incremented in small, uniform steps and the corresponding real valued index ( $i_{\text{new}}$ ) of 'i', are evaluated. Then the power contribution to each sample in 'j' is obtained by linear interpolation of the original power spectrum at the integer-valued indices that enclose  $i_{\text{new}}$ . The step size in 'j' has to be fine enough such that all samples in the original spectrum are utilized. A good choice for the step size is given by  $\Delta j = j(i = n_{\text{ch}}) - j(i = n_{\text{ch}} - 1)$  (5.17)

where the channels  $n_{\text{ch}}$  and  $(n_{\text{ch}} - 1)$  correspond to the high-frequency end of the observed band. In using linear interpolation, it is assumed that the phase rotation between two adjacent channels is small (say, less

than a radian) so that the interpolation error is small. Also, a separate log is to be maintained as to how many original samples were added to each bin in the linearized domain, so that the linearized data may then be normalized by the respective counts. The effective number of original samples contributing to each bin may be calculated alongside equation(5.17), as

$$\begin{aligned} \text{NADD}_{\text{int}(j)} &= \text{NADD}_{\text{int}(j)} + (1 - \text{frac}(j)) \\ \text{NADD}_{\text{int}(j+1)} &= \text{NADD}_{\text{int}(j+1)} + \text{frac}(j) \end{aligned} \quad (5.18)$$

Step 2: Fourier Transformation:

The signal-to-noise ratio (SNR) in the observed spectrum may be poor, making it difficult to estimate the parameters of the modulation. After linearization one may use the convenience of Fourier domain processing to estimate them. In this method, the RF power spectrum corresponding to each longitude is (inverse) Fourier transformed to produce the corresponding auto-correlation function (ACF). Then the magnitude of the ACF is evaluated. This corresponds to the true auto-correlation function convolved with a “sinc” function, corresponding to the window over which the spectrum is available. The ACF is then scanned to find the location of the most significant peak other than the zero-lag component. Having located the peak in the auto-correlation domain, the frequency of the modulating patterns and hence the RM is estimated using the equations mentioned above.

Step 3: Estimation of Co-efficients : The magnitude of the peak corresponding to the modulation frequency in the ACF gives the corresponding  $A_1$ , value, while the corresponding value of the 'zero-lag' auto-correlation (first point) provides  $A_0$  value. The ratio of  $A_1$  to  $A_0$  yields the corresponding fractional linear polarization. A better method is to estimate  $A_0$  directly as

$$A_0 = \frac{1}{N} \sum_{i=1}^{N_{ch}} P_i \quad (5.19)$$

This value may then be subtracted from the RF power spectrum before computing the ACF so that the power due to leakage from the sidelobes of the zero-lag component of the ACF is insignificant. This helps to improve the accuracy in the estimation of the modulation frequency, particularly when it is not very high. The value of  $\phi$  is given by the phase at the peak of the ACF for each channel. The angle  $\theta$  at each of the wavelengths can be calculated using the estimated RM, from relation (5.1). Then, from equation(5.6), the intrinsic position angle  $\zeta$  is estimated at different longitudes. The centroid of the final pulse-intensity profile is calculated and the corresponding longitude is labeled as  $0^0$ , and the other longitudes are then labeled with respect to this point, knowing the number of samples within the period. The final results are in terms of the fractional polarization and position angles as a function of longitude.

### Error analysis:

The uncertainty in estimates of the parameters  $A_0$  and  $A_1$  are represented by the rms of noise in the ACF regions excluding the zero-lag and the location of the modulation feature. For large signal-to-noise ratio(SNR) cases, the uncertainty in the modulating signal phase (expressed in radians) can be simply expressed as the reciprocal of the SNR at the peak of the modulation feature in the ACF. However, a given phase value can be produced by a wide range of combinations of RM and  $\zeta$  values, hence it is difficult to

decouple the errors in RM and position angle. If the value of  $\zeta$  is known then the RM value can be refined using the observed phase information provided, the possible  $2\pi$  ambiguity is resolved. When the intrinsic position angle is not known, only the modulation "frequency", rather than the modulation "phase", can be used to estimate the RM as mentioned above. The error in RM resulting from uncertainty in estimation of the modulation frequency can be related to the signal-to-noise ratio, as shown below.

a) Effect of non-integer number of modulation cycles:

If the number of modulation cycles within the bandwidth is not an integer, then the modulation feature contribution will not be centred on one of the sampled points in ACF with nominal delay resolution ( $1/B$ ). This can lead to wrong estimates of the parameters. Depending on the resolution with which the main lobe of the "sinc" pattern is represented (decided by the number

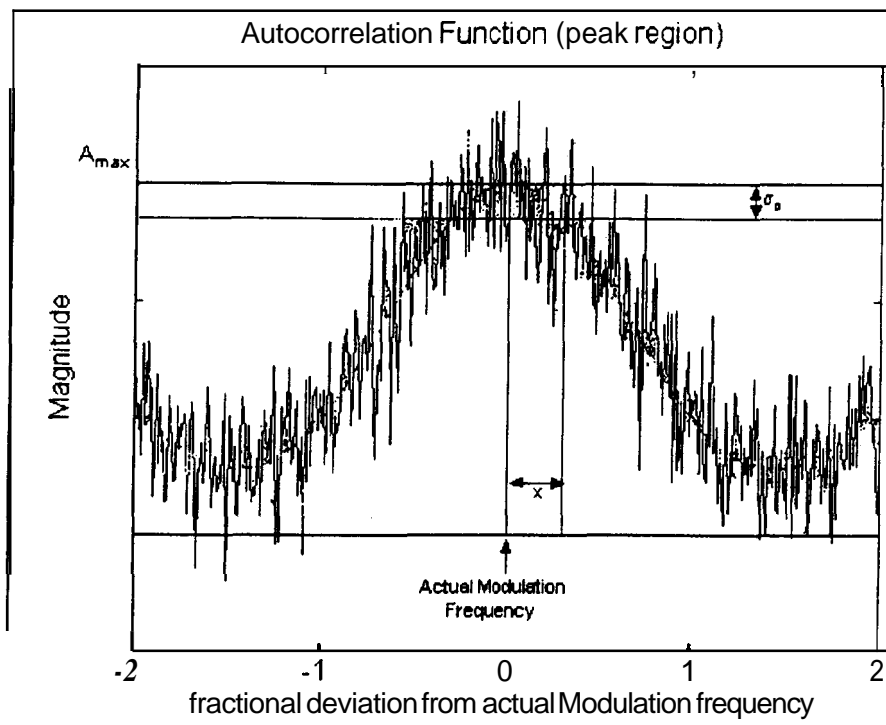


Fig. 5.2 Uncertainty in Modulation frequency due to Noise in Autocorrelation function

points in the sequence that is Fourier transformed), there will be an ambiguity in the identification of the location corresponding to the true peak of the feature. Finer sampling of the ACF improves the ability to detect the correct location of the peak, depending on the signal to noise ratio. This is achieved by oversampling of the ACF. Equivalently, this is achieved by padding a long sequence of zeros to the trailing edge of the measured spectrum, so that sampling interval in the ACF is much finer compared to the width of the main lobe of the sinc function. However, the ultimate limit is set by the inherent noise associated with the signal, as shown in the illustration of figure (5.2). Depending on the amplitude of this noise, the location of peak will be uncertain, which in-turn results in an uncertainty in the RM estimation. Around the peak in the ACF (corresponding to the actual frequency of intensity modulation), the magnitude falls off as a function of the fractional distance  $x$ , given by

$$P_x = P_{\text{peak}} \left( \frac{\text{Sin}(\pi x)}{(\pi x)} \right) \tag{5.20}$$

where  $x$  is the displacement from the location of the actual peak, in units of nominal delay resolution in the ACF (i.e.  $1/B$ ). If the uncertainty due to noise in determination of  $P_{\text{peak}}$  is given by  $\sigma_p$ , then the corresponding uncertainty  $x$  in determination of the location corresponding to the peak in the ACF is related as

$$\sigma_{\text{peak}} = P_{\text{peak}} \left[ 1 - \left( \frac{\text{Sin}(\pi x)}{(\pi x)} \right) \right] \quad (5.21)$$

or

$$\left( \frac{\text{Sin}(\pi x)}{\pi x} \right) = 1 - \frac{1}{\text{SNR}} \quad (5.22)$$

where SNR is the signal-to-noise ratio at the peak, expressed as

$$\text{SNR} = \frac{P_{\text{peak}}}{\sigma_{\text{peak}}} \quad (5.23)$$

Noting that the delay index in the ACF also represents the number of modulation cycles in the RF power spectra, the uncertainty in the actual number of cycles of the modulation within the band is  $x$  cycles. Thus, from the signal-to-noise ratio, an estimate of the uncertainty in RM can be obtained as

$$\sigma_{\text{RM}} = \frac{x\pi}{c^2} \left[ \frac{1}{f_L^2} - \frac{1}{(f_L + B)^2} \right]^{-1} \quad (5.24)$$

Thus, in enhancing the sampling rate for the ACF by padding zeros as mentioned earlier, it is optimum to reach a sampling  $R = x$ , beyond which the accuracy of RM value cannot improve further. By optimizing on the number of padded zeros, the computation time can be reduced.

After the Fourier Transform the signal to noise ratio of the modulation component in the ACF (magnitude only) is better by a factor of about  $\sqrt{N_{\text{ch}} / 2}$  over that in the power spectrum, where  $N_{\text{ch}}$  is the number of channels in the linearized spectrum. While the magnitude of the peak in the ACF indicates the linearly polarized power, the phase at the peak indicates the phase of the modulating sinusoid. The phase of this feature changes at different longitudes within the pulse since the shifts in the modulating pattern in the spectrum corresponds to the polarization sweep of the pulsar.

b) Effects due to Scintillation modulations:

The interstellar medium may produce scintillations which show up as superposed random modulations in the RF power spectra. Correspondingly, the ACF will then have the true RM feature convolved with a "scintillation feature". This convolution results in a spread around the true feature in the ACF and reduces the signal to noise ratio in the ACF, thereby increasing the uncertainty of the RM value. For a given value of RM, the parameters  $\zeta$ ,  $A_1$ , &  $A_0$  are used to fit a curve at all frequency channels across the band. The mean-square error in the fit is given by

$$\overline{e_L^2} = \frac{1}{(N_{\text{ch}} - 3)} \sum_{i=1}^{N_{\text{ch}}} (\text{data}_{i,L} - \text{fit}_{i,L})^2 \quad (5.25)$$

where data  $(i,L)$  and fit  $(i,L)$  are the raw data and the fit values respectively, at a longitude  $L$  during the on-pulse region of the folded profile and  $N_{\text{ch}}$  is to total number of channels used in the fit. Under noiseless

condition, the  $\overline{e^2}=0$  for a perfect fit. But in practical observations, the data itself is noisy, so that even if the fit is "perfect", there are deviations between data and the fit corresponding to the random noise in the data. In such a case, the value of  $\overline{e^2}$  will ideally same as the variance  $\sigma_{on}^2$  of the noise in the data. The deviation of  $\overline{e^2}$  from the noise-variance in the data indicates an estimate of uncertainty in the **model** parameters, (like RM for example). By computing  $\overline{e^2}$ , the uncertainty in RM can be estimated as discussed above using,

$$SNR = \frac{P_{peak}}{\sqrt{\overline{e^2}}} \quad (5.26)$$

### 5.3 Non-Linear Least-Square Error Fitting Algorithm

In this approach, a complete least-squares fit solution is sought so as to perform matched filtering and obtain the best fit corresponding to  $A_0$ ,  $A_1$ ,  $\zeta$  and RM. At any **given** position angle  $\zeta$  within the pulse, the pulsar data is expected to show an intensity modulation across the frequency channels of the band, characterized by equation (5.3). This may be rewritten in the following form:

$$I_{obs} = A_0 + A_1(\cos [h+2\zeta]) \quad (5.27)$$

where  $h = 2 RM \lambda^2$  and  $\zeta$  is the intrinsic position angle. This can be split into three terms, as

$$I_{obs} = A_0 + A_1[\cos(h)\cos(2\zeta) - \sin(h)\sin(2\zeta)] = A_0 + A_c \cos(h) - A_s \sin(h) \quad (5.28)$$

where

$$A_c = A_1 \cos(2\zeta); \quad A_s = A_1 \sin(2\zeta) \quad \text{and the DC part is } A_0 \quad (5.29)$$

The estimate of each term in equation(5.28) can be extracted by cross-correlating the observed intensity spectrum  $I_{obs}$  with respective functions (DC,  $\cos(h)$  and  $\sin(h)$ ) as follows :

The cosine part is given by

$$I_c = \frac{1}{N} \sum I_{obs} \cos(h) \quad (5.30)$$

Expanding

$$I_c = A_0 C_1 + A_c C_2 - A_s C_3 \quad (5.31),$$

where

$$C_1 = \frac{1}{N} \sum \cos(h); C_2 = \frac{1}{N} \sum \cos^2(h); C_3 = \frac{1}{N} \sum \cos(h)\sin(h) \quad (5.32)$$

The sine part is given by

$$I_s = \frac{1}{N} \sum I_{obs} \sin(h) \quad (5.33)$$

Expanding,

$$I_s = A_0 S_1 + A_c S_2 + A_s S_3 \quad (5.34)$$

where

$$S_1 = \frac{1}{N} \sum \sin(h); S_2 = \frac{1}{N} \sum \cos(h) \sin(h); S_3 = \frac{1}{N} \sum \sin^2(h); \quad (5.35)$$

The DC terms is obtained as:

$$I_d = \frac{1}{N} \sum I_{obs} \quad (5.36)$$

Expanding,

$$I_d = A_0 D_1 + A_c D_2 + A_s D_3 \quad (5.37)$$

where

$$D_1 = 1; D_2 = \frac{1}{N} \sum \cos(h); D_3 = \frac{1}{N} \sum \sin(h); \quad (5.38)$$

Noting that  $C_1 = D_2; C_3 = S_2; S_1 = D_3$ ,

the three equations for  $I_c, I_s$  &  $I_d$  can be solved simultaneously to give

$$\zeta = \frac{1}{2} \cos^{-1} \left[ \frac{1}{\sqrt{1+T^2}} \right] \quad (5.39)$$

$$A_1 = \frac{X \sqrt{1+T^2}}{(C_2 - C_1^2) - T(S_2 - S_1 C_1)} \quad (5.40)$$

and

$$A_0 = I_d - \frac{A_1 (C_1 - T S_1)}{\sqrt{1+T^2}} \quad (5.41)$$

where

$$X = I_c - I_d C_1; Y = I_s - I_d S_1; R = \frac{X}{Y}; T = \frac{(C_2 - C_1^2) - R(S_2 - S_1 C_1)}{(S_2 - S_1 C_1) - R(S_3 - S_1^2)} \quad (5.42)$$

The above derivation assumes a given value of RM. Using these parameters a new waveform may be generated and compared with the actual data, and the mean square error  $\overline{e^2}$  may be obtained for several trial values of RM in fine enough steps. The best estimate of RM corresponds to the fit with minimum  $\overline{e^2}$ .

### Error analysis :

The  $\overline{e^2}$  value depends on the correctness of the model, as well as on the other sources of uncertainty in the observed pattern. The standard uncertainty in each point of the observed pattern due to noise

associated with the signal is given by  $\sigma$ , which is also reflected in the calculation of  $\overline{e^2}$ . In the presence of modulations due to scintillations, the minimum  $\overline{e^2}$  is often larger than the rms of the inherent noise ( $\sigma$ ) due to the receiver and the sky. However, the variation of  $\overline{e^2}$  as a function of changes in the model-parameters (such as RM) can be used to estimate the standard uncertainty in the parameters values. In such a case, the change in  $\langle e^2 \rangle$  that is detectable which is equal to  $\langle e^2 \rangle / (N - N_{\text{param}})$  can be attributed to uncertainties in parameter values and the uncertainties of individual parameters can be derived after accounting for the degree of freedom. The minimum detectable change in the mean-square-error can be expressed in terms of the variance in individual parameters, to the first order, as

$$\Delta_e^2 = \frac{\overline{e^2}}{Nch - 3} = \frac{1}{Nch - 3} \sum_{i=1}^{Nch} \left[ \left( \frac{\partial I_{obs}}{\partial A_0} \right)^2 \cdot \Delta_{A_0}^2 + \left( \frac{\partial I_{obs}}{\partial A_1} \right)^2 \cdot \Delta_{A_1}^2 + \left( \frac{\partial I_{obs}}{\partial RM} \right)^2 \cdot \Delta_{RM}^2 + \left( \frac{\partial I_{obs}}{\partial \zeta} \right)^2 \cdot \Delta_{\zeta}^2 \right] \quad (5.43)$$

In the above relation, the covariances of the parameters are also to be considered, but are ignored for the sake of simplicity. Also, the entire error on the left hand side may be associated to one parameter at a time, to get the worst-case uncertainty in that parameter. Usually, the noise is of the same order in all the frequency channels. By considering one parameter at a time, the error may be related as follows:

For  $A_0$ ,

$$\frac{\overline{e^2}}{Nch - 3} = \frac{1}{Nch - 3} \sum_{i=1}^{Nch} \left( \frac{\partial I_{obs}}{\partial A_0} \right)^2 \cdot \Delta_{A_0}^2 = \sigma_{A_0}^2 \quad (5.44)$$

For  $A_1$ ,

$$\frac{\overline{e^2}}{Nch - 3} = \frac{1}{Nch - 3} \sum_{i=1}^{Nch} \left( \frac{\partial I_{obs}}{\partial A_1} \right)^2 \cdot \Delta_{A_1}^2 = \frac{\sigma_{A_1}^2}{Nch - 3} \sum_{i=1}^{Nch} \left( \cos \left[ 2(RM\lambda_i^2 + \zeta_i) \right] \right)^2 \quad (5.45)$$

For RM,

$$\frac{\overline{e^2}}{Nch - 3} = \frac{1}{Nch - 3} \sum_{i=1}^{Nch} \left( \frac{\partial I_{obs}}{\partial RM} \right)^2 \Delta_{RM}^2 = \frac{1}{Nch - 3} \sum_{i=1}^{Nch} \left( 2A_1 \lambda_i^2 \sin \left[ 2(RM\lambda_i^2 + \zeta_i) \right] \right)^2 \quad (5.46)$$

For  $\zeta$ ,

$$\frac{\overline{e^2}}{Nch - 3} = \frac{1}{Nch - 3} \sum_{i=1}^{Nch} \left( \frac{\partial I_{obs}}{\partial \zeta} \right)^2 \Delta_{\zeta}^2 = \frac{\sigma_{\zeta}^2}{Nch - 3} \sum_{i=1}^{Nch} \left( 2A_1 \sin \left[ 2(RM\lambda_i^2 + \zeta_i) \right] \right)^2 \quad (5.47)$$

The above method may yield reasonable estimate of uncertainties in RM and position angle when the RM is known with sufficient accuracy, so that there is no ambiguity in the associated phase in multiples of  $2\pi$ .

The maximum error that may occur when this condition is satisfied, is when the phase is in error by  $\pm \pi$ , and the corresponding maximum uncertainty in RM is then

$$(\Delta_{\text{RM}})_{\text{max}} = \frac{\pi}{2\lambda_L^2} \quad (5.48)$$

#### 5.4. Tests and Results:

The Auto-correlation domain processing method was evolved first and was tested on data of pulsar observations. As a first trial, the data of PSR 0740-28, a pulsar with reasonably large RM ( $\approx 150 \text{ rad m}^{-2}$ ) and pulse strength ( $S \approx 300 \text{ mJy}$ ), were obtained from ORT using the pulsar search preprocessor in April 1994, and were processed. The data in 256 frequency channels covering a bandwidth of 8 MHz around 327 MHz were aligned after correcting for dispersion delay gradient across the band, and folded over its period for about 10 minutes length of data, to improve the signal-to-noise ratio. The folded profiles of all channels were arranged in a matrix and the fit was performed at different on-pulse longitudes with zero padding, so as to have 32768 points in each spectrum. The estimated value of RM (which includes the ionosphere contribution also) is close to, but more than the quoted value of about 152 (Hamilton and Lyne, 1987). For a given SNR, the accuracy in estimation of the parameters is also limited by the fact that "linear" interpolation was used in sharing the power of original samples to those in the linearized domain. This also limits the modulation frequency that can be resampled properly, and thereby implies an upper limit for RM upto which good measurements can be made for a given bandwidth and operating frequency.

Figure (5.3) displays a 3-dimensional plot of intensity as a function of frequency and pulse longitude. Figure (5.4) shows the position angle, total (solid line) and linearly polarized intensity (dashed line) as a function of the pulse longitude. Figure (5.4 c) displays the profile of the same observation at 631 MHz, done with the 64-m antenna at Parkes, Australia (McCulloch et.al., 1978) for comparison. Comparison of the modulation pattern observed on three consecutive days (at a longitude selected at the peak of the pulse) shows a drift with respect to the frequency axis, indicating an apparent change in RM of about 0.5 day to day (shown in Figure (5.5)). The rate of change is too fast to be associated with the contribution of the interstellar medium, and is more likely to be due to changes in the RM of the ionosphere. This method and initial results were presented in a poster paper (Ramkumar & Deshpande, 1994). Subsequently, the non-linear fit method was developed and the tests were repeated for data from observations of the same pulsar (obtained in July 1997). The results of the two fit methods are shown in figure. (5.6). Figure. (5.6 a) shows the average  $A_0$  components obtained by the two methods, figure. (5.6 b) shows the fractional linear polarization  $dl$ , while the corresponding estimates of position angle are shown in figure. (5.6 c). Currently, the details of the above methods are being organized for paper publication.

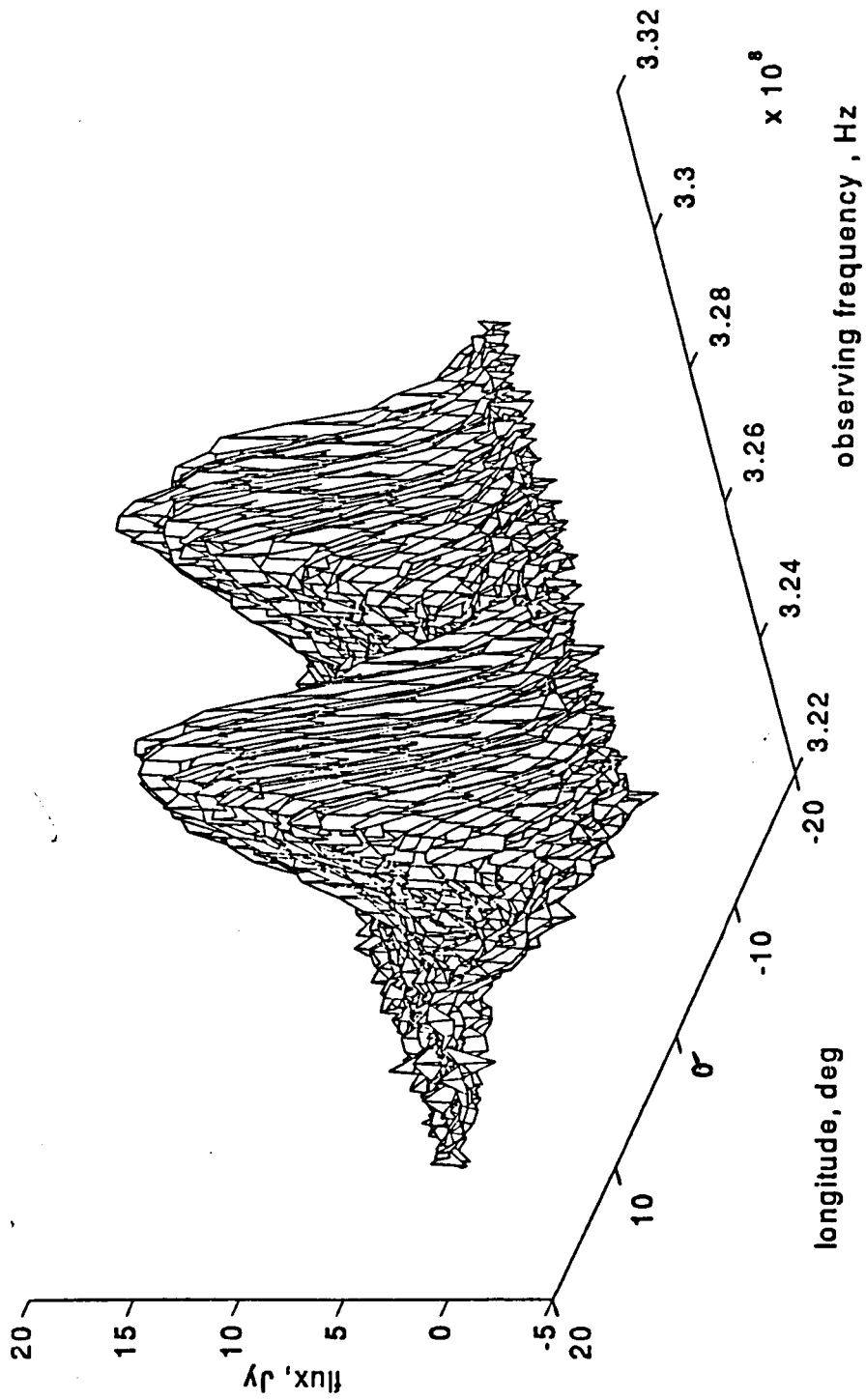


**Fig. 5.3** Pulse intensity as a function of frequency and the longitude (relative to the pulse centroid). Pulsar PSR 0740-28, observed on 19-03-94 at ORT using pulsar search pre-processor.

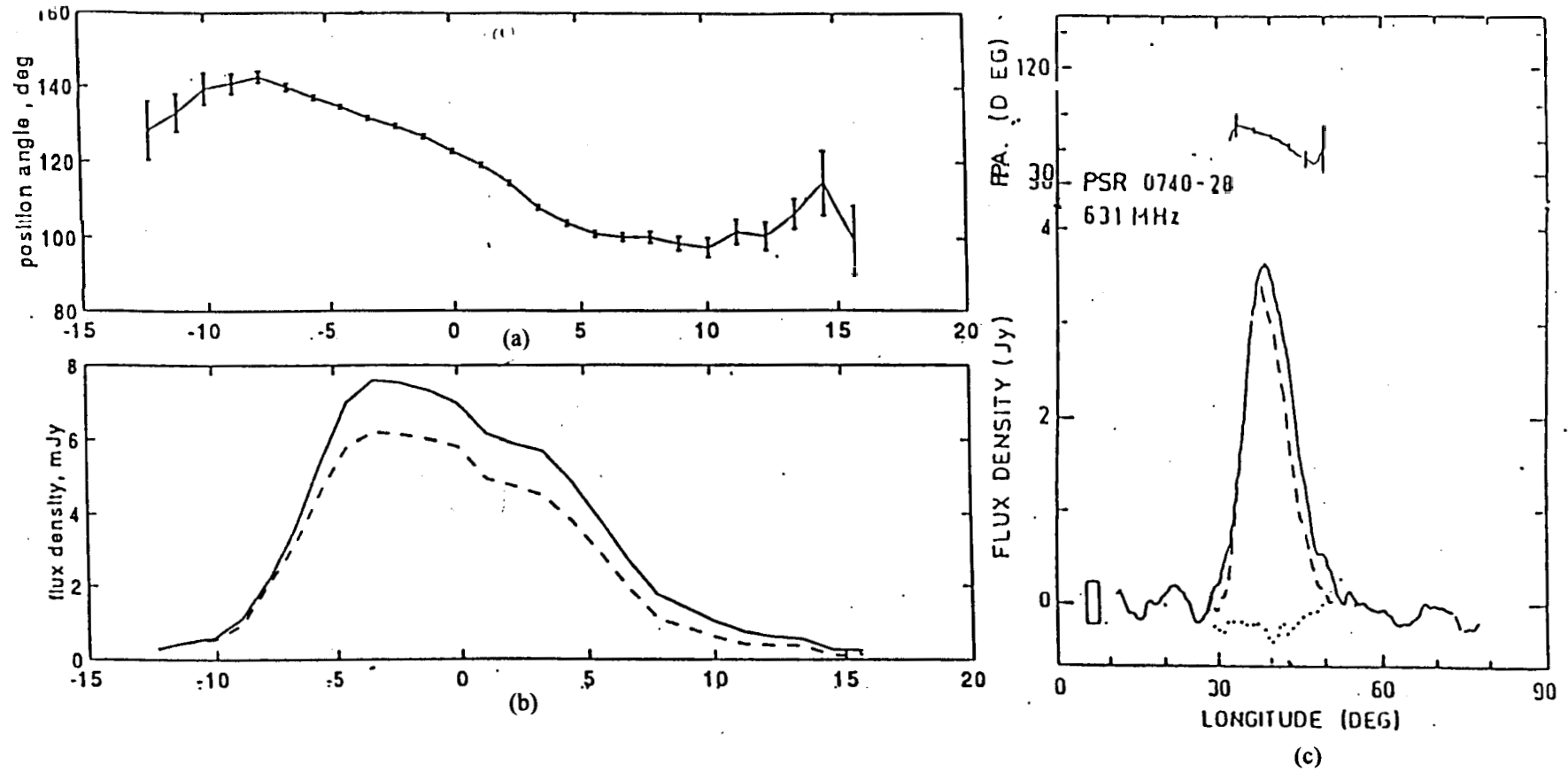
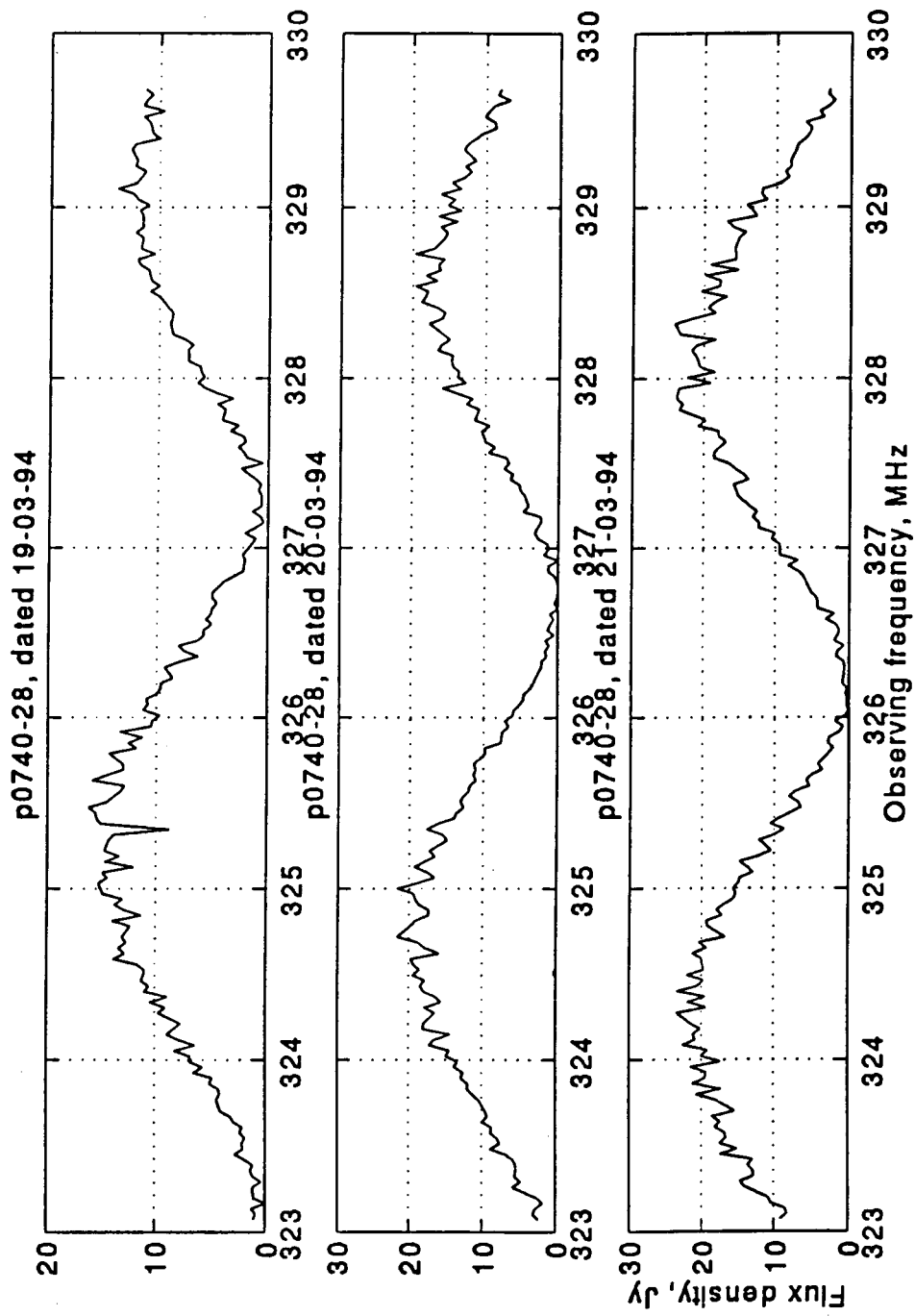


Fig. 5.4 Position angle (a) and Intensity profiles(b) as a function longitude. PSR 0740-28, observed on 19-03-94 at ORT using pulsar search Pre-processor. fig 5.4 (c) shows the profile of the same pulsar observed at 631 MHz using dual polarisation telescope by Mc Culloch et al, 1978.



**Fig 5.5** Average Power Spectrum showing modulations due to Faraday Rotation observed at the same pulse longitude on three consecutive days. A systematic drift can be observed in the modulation phase, possibly due to ionospheric RM Changes.

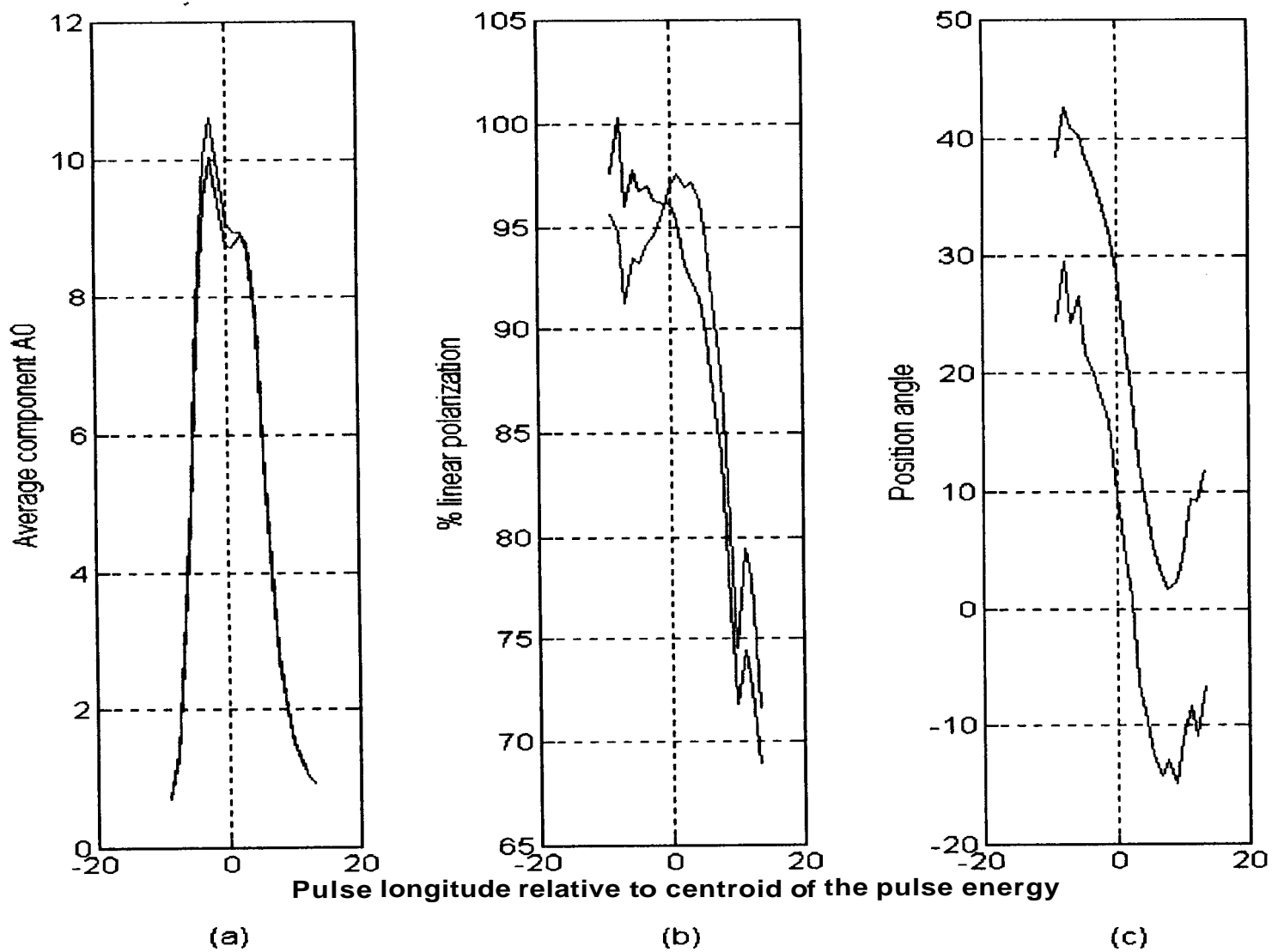


Fig. 5.6 Best-fit values of model parameters as a function of pulse longitude [ 'blue' lines indicate values obtained in Non-linear least-squares method (NLS) and the 'pink' lines are their counterparts obtained from Autocorrelation domain processing method (ACF)]. Source data from Pulsar PSR 0740-28, observed on 15 - 7 - 1997 (Peak SNR about 200). RM values obtained in fit : 153 (NLS) ; 152.3 (ACF) ; (Value quoted by Hamilton and Lyne, 1987 : 152).

## 5.5. Discussion

- In general, the bandwidth and the number of spectral channels set limits to the range for measurable RM, at a given operating frequency. The RM should be large enough to produce **at least** one cycle of modulation across the band, while it should be less than a value at which one cycle of modulation spans only two frequency channels. As mentioned in the first method, it is assumed that the rotation within two adjacent channels is much less than a radian, so that linear interpolation can be used without significant error. This assumption also imposes a limit on the minimum number of frequency channels over which the modulation can complete one cycle. In the second method, there is no such restriction and the fit is better. As such, these methods are well suited for observations of high RM pulsars or observations over relatively large bandwidths, where simple sinusoidal approximations to modulation phase may lead to significant errors in the estimation of RM. The FFT method does not need any initial guess of RM, while the NLS method is based on iterative trials for a range of RM values. In a practical case, it may be better to initially use the auto-correlation domain processing to arrive at an estimate of RM, and then use the non-linear fit method to refine the estimate. This will approach save the number of computations substantially, for measurements demanding high accuracy.
- The ultimate uncertainty limit for RM measurement is set by the signal to noise ratio of the data. In the ACF method, the SNR can be enhanced further by averaging the magnitude squares of ACF at different longitudes with appropriate weightages based on the pulse shape (ignoring the phase differences). The pulse longitude may be coarsely sampled, limited by the sweep rate of polarization angle within the pulse. Also, the folding length should be short compared to the typical time scales for apparent changes in the RM contributed by the ionosphere, so as to keep the depolarization due to integration well below the required RM accuracy. However, to smooth out the undesirable modulation due to interstellar scintillations it is desirable to average data over spans much longer than the de-correlation time scales of scintillation.
- The argument of the cosine term in the model may have the same value for a range of combinations of  $\psi$  and RM values. The ability to "distinguish between relative contributions from RM and  $\zeta$  terms improves as the bandwidth increases or operating frequency decreases, reducing the range of degenerate combinations of  $\psi$  and RM reduces. Since the estimated value of RM is "**weak**" function of the modulation phase ( $h + 2\psi$ ) the estimation is much higher for RM measurements. By the same argument, the prediction of the position angle of the radiation at the pulsar depends directly on the modulation phase from which the RM contribution is to be removed. Hence only rough estimates can be made since large changes in phase may easily be induced by very small changes in the RM value. On the other hand, the estimation accuracy of RM and  $\zeta$  is much higher in differential measurements, since the fit attributes any changes in the modulation phase to the parameter (RM or  $\psi$  respectively), Thus, the sweep of intrinsic position angle across the pulse (where RM is constant) and the changes of RM with time (where the intrinsic position angle is constant) can both be measured with high accuracy, since these are differential measurements.

- For a given signal to noise ratio, the non-linear least - squares fit method has better performance than the ACF method, since it uses the complete information (amplitude and phase) of the signal to fit for RM, while in the ACF method, only the amplitude information is used.
- A comparative study of such observations made on a given suitable pulsar on short time spans should provide useful information about ionospheric rotation measure change as a function of hour-angle and time in general. As such changes are expected to be small, they would noticeable first in the variation of the reference phase of the modulation cycle. This information should help us in modeling the changes in the ionospheric rotation measure reliably.

# CHAPTER SIX

## DISCUSSION & CONCLUSION

In chapter 1, a brief review of the characteristics of the pulsar signals and distortions caused to these signals due to propagation effects, relative motion of the Earth and pulsar and the instrumental response were presented. Conventional signal processing methods used to correct some of these effects were discussed. Various types of pulsar observations and relevant aspects of signal processing were reviewed. The front-end instrument available at the GMRT and ORT were briefly explained. Several optimizations to minimize the complexity in the signal processing methods to handle the real-time processing requirements for different types of pulsar observations were discussed in chapter 2. The details of implementation of the Pulsar Search Pre-processor (PSP) and the tests conducted using the system were presented in chapter 3 along with the results obtained. The details of the instrumentation for a Portable Pulsar Receiver (PPR) were also presented along with the results. The architecture of the polarimeter and a DSP parallel processing system which form the signal processor for pulsar studies were detailed in chapter 4. The strategies for distribution of the code & data and relevant optimizations in the implementation of the signal processing algorithms were presented. Implementation details of a high speed data recording system built for collecting results from SPPS was also explained. The design of a Fast Fourier Transform (FFT) module built for testing the SPPS was also explained. Tests conducted and results obtained were presented.

In the following discussion, the tests that may be conducted further are mentioned. Also, some simplifications are identified, that can be brought about in future designs by making use of some alternative implementation methods and the new developments in technology.

### 6.1. Present Status and Possible Improvements

#### 6.1.1. Pulsar Search Pre-processor (PSP):

- The PSP has been successfully working for pulsar observations at both ORT and GMRT. Even though the laboratory tests have ensured that the machine works well under all configurations, field observations hitherto have been limited to one-bit, IA mode, since this was the most suited configuration for the on-going pulsar survey. So far, the machine has been used in the same mode for pulsar survey, pulsar timing observations and some calibration experiments on various sub-systems of the GMRT. Test observations with gain calibrated band-shape are currently underway at ORT using the PSP in the two-bit mode. Once the PA mode of GMRT becomes available, the system can be used to conduct targeted search and study of Pulsars.

- The running mean evaluation logic may be simplified by using a first order recursive filter of the form

$$M_{(i)} = \frac{[M_{(i-1)} \cdot (N - 1)] + d_i}{N}, M_0 = 0, i \geq 0. \quad (6.1)$$

where M is the mean after the 'i' th block integrated sample and N is the desired smoothing interval of the filter in units of the number of block integrated samples. With this impulse response, a fresh sample of a block-integrated value gets the greatest weightage in the evaluation of the mean and its subsequent contribution to mean of previous samples gets reduced exponentially. This will result in a frequency response with a significant reduction of sidelobes, consequently reducing the leakage of power from the pulsar signal to the estimated mean. The implementation will need only 256 locations (one per channel) will be needed to hold the running mean of all frequency channels, and will also provide a simpler implementation with 32-bit accumulators, without the involvement of the control PC in evaluation of the running mean. Given the bit-width and speed of currently available logic, the accumulators may update the running mean at the same rates as that of the pre-integrated data.

- With the advancement of VLSI technology, the EPLD/FPGA devices have significantly improved in their performance (propagation delays have reduced from about 25 ns to 10 ns and gate densities have increased from about 2000 to 100,000 gates). Additionally, the latest devices are available with on-chip, re-configurable memory, upto about 24 kbits. As such, the entire circuit designed for the PSP can be hosted into a single FPGA device in future reproduction, which will be cheaper and consume lesser power, besides saving space and providing more flexibility.

### 6.1.2. Polarimeter :

- Ever before the phased-array mode of GMRT becomes fully operational, the polarimeter module can provide useful information about the cross-polarizations, inter-channel leakage, degradations due to antenna deformations, etc. by tapping the dual polarization channels of individual dishes of the array separately. This test would begin soon.
- It is necessary to maintain an account of the number of input samples added to each of the time bins in the average profile for a given number of integrations/folds for each block of resultant data recorded. This information is important for normalizing the results with appropriate weightages during post-processing. In order to provide this information without using an 'extra' array for these counts in the current system, a carrier signal is injected at a fixed power level and frequency (set to appear at the edge of the band, preferably). The deflection counts in the channel corresponding to the carrier signal is measured initially. When the DSP processor routine integrates/folds the data of individual channels while observing a known pulsar. the growth of counts in the different time bins of the profile corresponding to the carrier channel is proportionate to the number of samples added to corresponding bins. However, a more stable and simpler method would be to replace the data samples of a chosen channel with pre-programmed (constant) digital numbers ('marker'), at the point where the Stokes parameters are computed and distributed across nodes.

The digital marker pattern is assured to be a constant number and can be used in a similar fashion as mentioned above. Depending on the portion of the band being processed, the 'marker' data may have to be injected on a different channel. This facility is provided in the revised version of the Polarimeter, which will be used for further work.

- With the availability of new **FPGAs** mentioned above, it has become possible to host the entire polarimeter (Stokes parameter generation and data distribution) circuitry in a single, 100,000 gate device, including the associated memories. With faster **buffer/line** driver chips available at high density and small outline surface-mount packages, it has become possible to accommodate transmission of all stokes parameters to all nodes on a single bus, at higher speed. The revised version has been tested under simulation to work successfully at the required speed. This has resulted in significant reduction in the space, PCB routing complexity and cost of implementation. In addition, the correction step for Faraday rotation has also been imported from the DSP algorithms into an equivalent hardware realization inside the same FPGA chip, thus simplifying the job for the DSP (this correction is a dedicated calculation, and the saved DSP time can be utilized for more intelligent tasks).
- In the present system, the organisation of the data path is hard-wired to the nodes and there is no easy way of reallocating the nodes to handle different portions of the band. During the design of the above mentioned chip, a facility has been incorporated to be able to send any group of 32 channels to any node.
- The GMRT front-end system (Sampler, FFT, etc) has been designed to work at a fixed speed of 32 Msamples per second, irrespective of the chosen base-band width. This results in over-sampling for smaller band-widths, and depending on the chosen bandwidth, the **FFT** spectra may provide **semi-redundant** information for several timeframes. A facility has been incorporated in the revised design mentioned above, so as to periodically skip a programmable number of **FFT** spectra that arrive from the array combiner, so as to utilize the available time more efficiently.

### 6.1.3. DSP Parallel Processor :

- As mentioned in chapter 4, the DSP nodes process the results and store them in their respective secondary **SRAMs (SRAM-Bs)**. The Data recording system is expected to send the addresses of the corresponding locations and read out the results from each node for storage. While this scheme works perfectly well, it is simpler to realize the same secondary memory in form of a set of **FIFO** memory chips, so that the address generation can be avoided on both sides of this memory (since, the data storage system always reads out the results sequentially). This reduces the routing complexity and probable cross talk on the system bus. The cost of high-density **FIFO** chips has reduced and it is feasible to realize the above scheme at prices similar to those of equivalent SRAM modules. This improvement is adopted in the revised DSP boards.

- The assembly code written for TASK2 can be parallelized for saving time during the interval when the FIFOs are yet to fill, and this time can be utilized for realizing additional operations such as gating with multiple windows to handle pulsars profiles having interpulses. Also the DSP software can be upgraded to automate the process of peak detection and window positioning within the profile in each node. This requires that the DSPs initially fold the data, collapse all channels and search for any deviations significantly beyond the mean level in the profile. Upon detection, the corresponding location can be identified and a window can be set around the peak to a user-specified width. This technique is yet to be tried out during actual pulsar observations.
- Without major hardware modifications, the SPPS system can be used to obtain coherent de-dispersion on raw data samples. The polarimeter will then have to tap the raw voltages from the sampler (instead of reading out from the FFT modules) and deliver the stokes parameters to the DSP nodes. The bandwidth that can be handled by the DSP parallel processor may be lesser in this mode (about a few MHz), but will be very useful for high time-resolution studies of pulsars. Additional signal processing software will have to be written in this case.

#### **6.1.4. Data Recording System :**

- In the present design, even though the number of DSP nodes and the sequence in which the results are to be read out can be specified in the DCS, there is a possibility that if a node fails to respond when the DCS expects it to provide results, the DCS will hang waiting for response from that node. To handle such a situation. the revised DCS module is equipped with a time-out mechanism (in case the current node accessed does not indicate its readiness for result transfer within a preset interval of time) which will prompt the controller to move on to the next node in the specified list and sequence.
- The DCS registers and FIFOs are memory mapped in the area D0000 to DFFFF (hex) and interfaced via the ISA bus of the IBM PC-AT. With the recent advancements in the PC/AT architectures, PCI bus is taking over as a standard, Windows operating system is replacing DOS systems and the free memory region available for mapping user-defined cards is being relocated to higher memory addresses. Considering the fast rate of changes in the architectures in the recent past, it may be better to have a small add-on card with minimal logic (just enough to handle the BUS signals for handshaking) and have the rest of the DCS logic on a separate platform, so as to be able to easily switch from one PC platform to another. With this in view, the revised DCS has the ISA bus interface built on a small buffer-card, and the rest of the DCS logic has been imported into the same FPGA chip mentioned above, which also hosts the polarimeter.

#### **6.2. Scope for other Applications:**

Even though the system is designed primarily for pulsar observations, many parts of the system may be useful in some other applications. In the following discussion, only some applications that are readily apparent are mentioned, while there may be many that may be possible. The applications may not render

themselves feasible readily, and may need minor modifications in the hardware/software of some modules to adapt it to the application.

- Presently, the interconnections in the back-plane between the nodes are hard-wired into a tightly coupled architecture. The SRAM-Bs on all nodes is being used only for uni-directional communication, namely, for outputting results. By using a suitably modified back-plane and a bus-management processor, the full features of a loosely coupled parallel processor can be tapped. In this mode, the nodes can access each other's **SRAM-B** memories for exchange of data and messages. The architecture of such a new back-plane has been developed and the associated protocols have been simulated in software, using a **lower-end DSP chip (ADSP 2101)** to handle the bus-management. In this method, any node can apply for the **BUS** to interact with any other node, and the controller keeps such requests in a queue and services the requests on a programmable priority basis through suitable handshake signals with the concerned nodes. By this method, the overall memory available across all the nodes can be used more efficiently as a common distributed resource. The simulations have shown that the maximum latency for switching the connections between nodes may be less than a microsecond and it is more efficient to use block-transfers of data. With efficient programming, the parallel processor can deliver a peak computational power of about 1 Gops with sixteen nodes. However, as in any parallel-processing paradigm, the efficiency depends on the suitability of the problem to the parallel processor, and the available power may not always be usable at its maximum. This system is a useful, general-purpose signal processing tool that can handle a variety of jobs which need intensive computing.
- The PC add-on DCS system can be used for any other general digital-data acquisition application. During the design and development of this module, several alternative schemes were tried out. The same logic was also interfaced on EISA (Extended Industry Standard Architecture) **PC/AT** bus, in which 32 bit data transfers could be made to the hard-disk controller. The maximum data recording rates achievable (with 32K x 16 bit **FIFOs** to buffer the data) was about 256 **Kbytes/sec** on the ISA interface and about **1Mbytes/sec** on the EISA interface. The speed and the data storage capacity are limited by the **latency/seek-time** and the size of the hard disk.
- The polarimeter can be used independently to obtain the cross-correlation and auto-correlations of any two complex quantities, represented in the appropriate format. The polarimeter module can run at speed **upto 20 Msamples per second** and, in the revised version, it is available in a single EPLD chip.
- Different diagnostic circuits that were developed as test-jigs for this instrument will be useful, in general, as a PC-based debugging tool for any digital circuit which runs within a speed limit of about 16 Msamples per second. Apart from the simple EPLD-based pattern generators, the design has been extended to provide programmable patterns that simulate dispersion, Faraday rotation, etc. with the help of a state sequencer and a large pattern memory (**64Kx64**). This can be used as a 64-bit pattern sequence extending **upto 64K states**, and can be read out in any sequence. A 196-line parallel **I/O** module has also been developed to set control signals, static data and read back results, from a PC platform. This would

be very useful in debugging circuits at speeds ranging from single-step mode to about 8000 **states/sec**. A PC-based, 12-digit frequency counter has also been developed to measure the frequency of the device under test, with the help of a stable external reference oscillator. The accuracy of measurement is limited only by the chosen reference oscillator.

- To provide the capability of fast coherent de-dispersion on the **portable-pulsar** receiver system, the Plessey FFT module was adapted to the **PC/AT EISA** bus architecture, to provide an accelerator, which can be used as a PC add-on, memory mapped module. With this, the same PC which would acquire data from the PPS during an observation may be used to quickly analyse the data. The main computational load comes from coherent de-dispersion which needs **FFT** of long stretches of data (about a million samples). Software routines written in C and tried on a **Intel 486 PC/AT** operating at 66 Mhz could produce the required transforms in about 1 minute, while the same computations could be performed by using the **FFT** accelerator within about 3 seconds. This speed limit is only due to the limitations of the bus, and the same mechanism can be easily adapted to any other bus standard with a suitable interface, so that the computations can be realized much faster. The ultimate limit imposed by the **FFT** hardware is much faster, about 0.1 seconds for the same job.
- The technique of linearization used in the ACF fit method is useful in some other applications where a non-linear function has to be resampled into a linear domain. The same technique was tried in two more applications concerned with post-processing for pulsar search observations:
  - a. The data will be **resampled/corrected** for several trial values of Doppler acceleration before trying the routine search processing for a significant detection. In such a case, the change in the apparent pulse-period is a non-linear function of time. The same method can be adopted to **compress/expand** the profile such that the pulse-phase is always arranged in linear progression, for further processing.
  - b. During de-dispersion, the data of different frequency channels will have to be added after compensating the delay gradient corresponding to a given DM. Several trials have to interact with different DM values, to identify the best fit. The dispersive delay is a non-linear function of frequency. It is possible to linearize the apparent delay gradient by resampling the frequency spectrum at suitable non-linear intervals in frequency, using the same linearization method. This linearization helps in simplifies the de-dispersion operation, since it is then possible to assume that the pulse phase-offset from one channel to another is constant.
- The technique described in chapter 5 can be fruitfully employed to make new rotation measurements on a large number of pulsars. The high degree of accuracy obtainable in the measurement of RM by including the pattern phase information has attractive applications in monitoring of the ionospheric RM and changes in the RM of pulsar with earlier epoch measurements. This method can be used with other telescopes possessing sufficient collecting area to conduct systematic monitoring of changes in the

electron-density and the magnetic field orientation in different regions of the ionosphere, the solar Corona and the interstellar medium in general.

### **6.3. Summary :**

The PSP and SPPS are working satisfactory in the field according to the design specifications. The current PSP can handle the full 32 MHz band-width of GMRT, and most of the improvements mentioned above will be incorporated in the system. The SPPS system is currently equipped with two DSP nodes so as to handle a total of 4 MHz band-width. The system will be enhanced to handle the full 32 MHz band-width by reproducing more DSP nodes. Some refinements mentioned above already are being incorporated in this final and full system which is under production currently. The RM measurement methods have given successful preliminary results and will be used for new RM measurements of pulsars and monitoring of the intervening medium.

**The work presented in this thesis described the details of the design and development of a major component of the pulsar instrumentation for the GMRT. With the addition of these digital back-ends, the GMRT would become a competitive observing facility for pulsar research.**